Songklanakarin J. Sci. Technol.
40 (3), 623-632, May - Jun. 2018

http://www.sjst.psu.ac.th

Original Article

Experimental and numerical study of the solidification process in saturated porous media: Influence of the solid particle, types and freezing temperature

Wirasak Khongkaew, Chayanon Serttikul, and Phadungsak Rattanadecho*

Center of Excellence in Electromagnetic Energy Utilization in Engineering,
Department of Mechanical Engineering, Faculty of Engineering, Thammasat University,
Rangsit Campus, Pathum Thani, 12120 Thailand

Received: 16 November 2016; Revised: 20 February 2017; Accepted: 12 March 2017

Abstract

This research conducted an experimental and numerical study of the solidification process of a water saturated porous medium. The experiments were conducted in a rectangular test cell cooled from the lateral walls to obtain quantitative temperature distribution and solidification interface motion. Solid glass and steel particles were used as the porous medium and distilled water was the phase-change material. A one-dimensional mathematical model considered heat conduction as the only mode of heat transfer in both the frozen and unfrozen layer. A comparison of the experimental data with numerical predictions of the interface position and temperature distribution showed good agreement and thus confirmed the proposed mathematical model for a system of glass particles and water. For a system of steel particles and water, the computed results give the same trends as the experimental data.

Keywords: numerical simulation, coordinate transformation, saturated porous media, solidification process, solidification interface

1. Introduction

The phenomenon of the solidification process in saturated porous media occurs widely in nature and in many engineering systems. Some of the specific applications include crude oil transport in permafrost regions, transportation of coal in cold weather, formation of ice on vehicles and structures, solidification of alloys or crystals, food processing, chemical processes, and cryopreservation of engineered tissues.

Many problems for simultaneous heat and mass transfer in porous media have been studied by many authors including: Weaver and Viskanta (1986); Beckermann and and Viskanta (1988); Chellaiah and Viskanta (1989); Ng and Mujumdar (1998); Zhang and Hung Nguyen (1999); Ismail and Henríquez (2000); Rattanadecho *et al.* (2001); Devireddy *et al.* (2002), and Lu and Zhou (2002). Apart from the above, Javierre *et al.* (2006) consi-dered the convenience of numerical techniques and the accuracy of results by a comparison between many numerical models and analytical solutions. Serttikul and Rattanadecho (2007) studied the numerical analysis of the melting process in phase change materials. The variable space grid technique was combined with the finite difference method to solve the results for prediction. Olguin *et al.* (2007) studied the free boundary of the Stefan problem by changing the thermal coefficient of the substance with the finite difference method and compared it with many methods from the exacted solutions. Rattanadecho and Wongwises (2008) considerated the moving boundary-moving mesh of a freezing process using combined transfinite interpolation and the partial differential equation mapping method. Sathaporn *et al.* (2008) researched the phenomena of melting ice slurry on the external surface of a copper helical coil and studied the influence of the coil diameter. Tan (2008)

*Corresponding author
Email address: ratphadu@engr.tu.ac.th

studied the melting of phase change material inside a sphere using *n*-octadecane for both constrained and unconstrained melting at different temperatures. Seeniraj and Sankara Hari (2008) investigated the freezing of liquids in forced flow inside convectively cooled tubes with the transient problem. Hosseini (2012) showed experimental and numerical data in a study of buoyancy driven flow during the melting process. The effect of inlet temperature of the fluid was investigated. Rattanadecho *et al.* (2014) reported the numerical and experimental analysis of heat transport and water infiltration in a granular packed bed due to hot water to predict the infiltration shape of hot water by gravity. Hao *et al.* (2014) presented the application of the moving mesh method for two-phase flow in porous media. It is used to distribute more mesh near the interface to improve the efficiency and accuracy of the result.

Only a limited amount of experimental work has been reported on heat and mass transport with saturated porous media. Therefore, insight of the phenomenon is incomplete. In dealing with the moving boundary problem, i.e. the solidification process of saturated porous media, a complication arises due to the motion of the solidification interface with the phase transformation. The position of the interface is unstable within the domains over which the heat transport varies. The purpose of this work is to systematically conduct the numerical and experimental studies of the freezing process in a saturated porous media. This study focused on different types of solid particles and freezing temperatures on the solidification interface and temperature distribution during the freezing process in saturated porous media.

2. Experimental Apparatus

Figure 1 shows the apparatus where the solidification experiments were performed which included a rectangular test cell with inside dimensions of 130 mm height, 110 mm length, and 50 mm depth. All test cells were made from acrylic resin. All sides of the test cells were covered by 60 mm thick Styrofoam to protect the effect of heat loss and condensation of moisture at the walls. The cavity of the test cell was filled with a mixture of water and uniform size spherical beads (0.15-mm diameter) to serve as the porous matrix. The heat source was provided at the vertical front wall from a multi-pass heat exchanger. The heat exchanger was connected through a system of valves to a constant temperature bath, where an ethylene glycol–water solution was used as the coolant solution. Throughout the experiments, the test cell was set up at a constant room temperature of 10 °C. Temperature distributions in the test cell were measured using Cu–Co thermocouples (0.6 mm diameter). All thermocouples were positioned to measure along the horizontal center plane in the test cell at 10-mm intervals. The thermocouples were connected to the data logger which measured and stored the temperatures at preselected time intervals. The position of the solidification interface in the test cell was determined by interpolating the fusion temperature from the thermocouple recording.

Figure 2 shows the test cell of the solidification process. Heat exchange was at freezing temperatures of the phase change material in a packed bed that consisted of two layers: frozen layer (1) and unfrozen layer (2). The solidification interface moved to all positions of the thermocouples along the horizontal center plane of the test cell. Finally, a comparison was performed of the behavior of solidification between the numerical results and the experimental data.

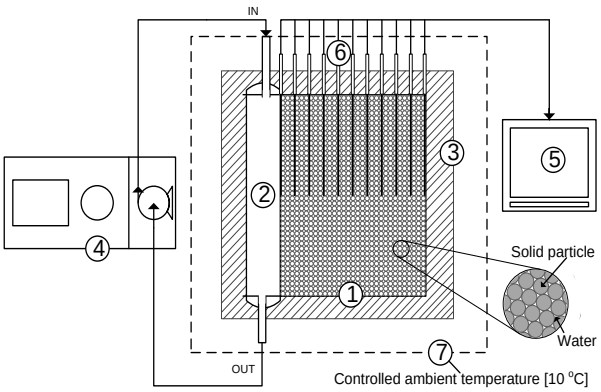

Figure 1. Experimental apparatus: 1) test cell, 2) cooling heat exchanger, 3) insulator, 4) cooling tank with refrigerator, 5) recorder, 6) thermocouples, and 7) control room.

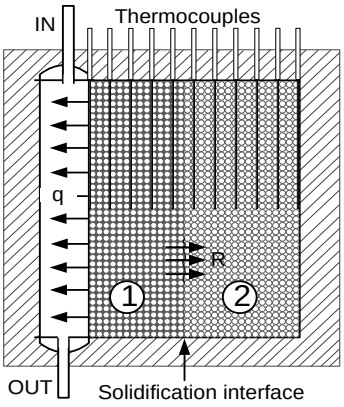

Figure 2. Test cell.

3. Analysis of the Solidification Process in the Saturated Porous Media

In Figure 3, the physical model consisted of two layers, namely the frozen layer and unfrozen layer. Inside the frozen layer, only heat transport took place, whereas inside the unfrozen layer both heat and water transport occurred. Initially, the system was at a uniform temperature greater than or equal to the fusion temperature of the liquid. At time $t > 0$, a uniform temperature less than the fusion temperature was imposed on the left wall. Solidification was initiated at this wall and the solidification interface moved from left to right. The following simplifying assumptions were made in the analysis:

1. Analysis of the solidification was in a saturated granular packed bed of one-dimensional. The solidification interface was planar for good control of the temperature gradient in the experiment.

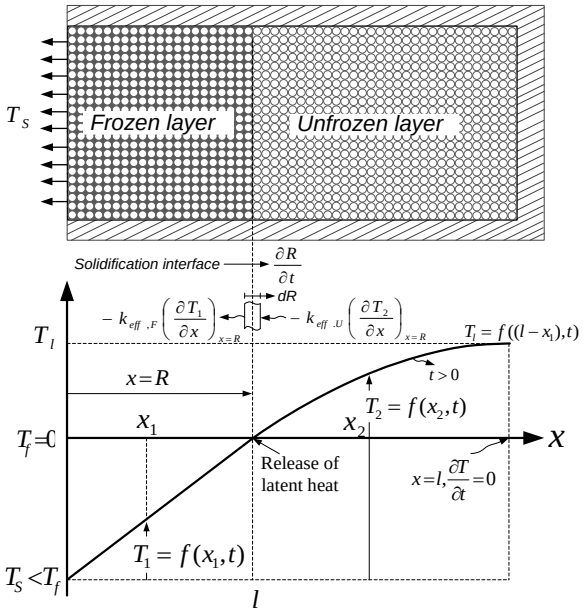

Figure 3. Physical model for solidification process.

2. The energy balance equation was considered at the solidification interface which predicted the position of the solidification interface. It was based on an energy balance of an infinitesimal control volume along the planar interface.
- The uniform porosity of the porous media was isotropic and homogeneous. Therefore, the volume of the average model for isotropic and homogeneous material could be used in the theoretical and analysis.
3. Volumetric change from solidification was negligible.
4. Natural convection was absent.
5. The frozen–unfrozen interface was clearly defined, i.e. the phase-change material had a well-defined fusion temperature.
6. The thermal equilibrium condition between the phase-change material and the porous matrix was considered. This may occur when the porous matrix had a slightly larger thermal conductivity than the phase change material, and hence the interphase heat transfer could be properly neglected.

The energy conservation equations in the frozen and unfrozen layers are given, respectively, by the following equations.

In the frozen layer (ice + solid particle)

$$\left\langle \rho C_p \right\rangle_{eff,F} \frac{\partial T_1}{\partial t} = k_{eff,F} \frac{\partial^2 T_1}{\partial x^2} \tag{1}$$

and in the unfrozen layer (water + solid particle)

$$\left\langle \rho C_p \right\rangle_{eff,U} \frac{\partial T_2}{\partial t} = k_{eff,U} \frac{\partial^2 T_2}{\partial x^2} \tag{2}$$

where $\left\langle \rho C_p \right\rangle_{eff}$ is the effective heat capacitance of the water or ice and matrix mixture and k_{eff} is the effective thermal conductivity which depended on the water or ice saturation. Under the thermal equilibrium condition, the effective heat capacity is given as

$$k_{eff} = \varepsilon k_{ice\ or\ water} + (1-\varepsilon) k_{solid\ particle} \tag{3}$$

$$\left\langle \rho C_p \right\rangle_{eff} = \varepsilon \left\langle \rho C_p \right\rangle_{ice\ or\ water} + (1-\varepsilon) \left\langle \rho C_p \right\rangle_{solid\ particle} \tag{4}$$

The solidification interface was caused by the mechanism of phase changes in the material which was the energy fed into the system converted to latent heat used for phase change from the liquid to solid state. The motion of the frozen layer or solidification interface is represented by

$$L\rho\varepsilon \frac{dR}{dt} = k_{eff,F}\left(\frac{\partial T_1}{\partial x}\right)_{x=R} - k_{eff,U}\left(\frac{\partial T_2}{\partial x}\right)_{x=R} \tag{5}$$

The initial conditions and the boundary conditions are:

Initial conditions

- Positions $x > 0,\ t = 0,\ T_1 = T_0 =$ constant

Boundary conditions

- Positions $x = 0,\ t \geq 0,\ T_1 = T_S$
- Positions $x = l = 0.1\ m,\ t \geq 0,\ \frac{\partial T}{\partial x} = 0$
- Positions $x = R(t),\ t > 0,\ T_1 = T_2 =$ constant $= T_F = 0$

4. Coordinate Transformation

To order solve the moving boundary problem that includes phase change phenomena, complications arise due to the motion of the evaporation front with elapsed time. In this study, the governing equations for water and heat transport were solved using a coordinate transformation technique based on the boundary fixing method coupled with an implicit time.

4.1 Coordinate transformation in the frozen layer

For the coordinate transformation in the frozen layer, the following coordinate system is

$$\eta = \frac{\mathrm{x}}{R(\mathrm{t})}, \qquad 0 \leq \mathrm{x} \leq R(\mathrm{t}) \tag{6}$$

where R(t) is the distance between the heated surface and the solidification interface. By using this coordinate system, the physical space $f(x,t)$ is transformed to a mapping space $(f(\eta(x,t),t))$. The differential operators with coordinate transformation are mathematically related through the following equations (Farrashkhalvat & Miles, 2003; Rattanadecho, 2008):

$$\frac{\partial}{\partial x} = \frac{\partial}{\partial \eta}\frac{\partial \eta}{\partial x} = \frac{1}{\mathrm{R}}\frac{\partial}{\partial \eta} \tag{7}$$

$$\frac{\partial}{\partial t} = \frac{\partial}{\partial \eta}\frac{\partial \eta}{\partial t} + \frac{\partial}{\partial t} = \frac{\partial}{\partial \mathrm{t}} - \frac{\eta \dot{R}}{R}\frac{\partial}{\partial \eta} \tag{8}$$

where $\dot{R}$ denotes the time derivative of the evaporation front location. Corresponding to Equations 7 and 8 after some mathematical manipulations, the energy transfer equation in the frozen layer (Equation 1) can be transformed.

$$\left\langle \rho C_p \right\rangle_{eff,F}\frac{\partial T_1}{\partial t} = \left\langle \rho C_p \right\rangle_{eff,F}\frac{\eta \dot{R}}{R}\frac{\partial \mathrm{T}_1}{\partial \eta} + \frac{k_{eff,F}}{R^2}\frac{\partial^2 T_1}{\partial \eta^2} \tag{9}$$

4.2 Coordinate transformation in the unfrozen layer

The following coordinate transformation is utilized in the unfrozen layer:

$$\varsigma = \frac{\mathrm{x} - R(\mathrm{t})}{l - R(t)}, \qquad R(\mathrm{t}) \le x \le l \tag{10}$$

where l denotes the total length of packed bed. Also, in using this coordinate system, the physical space $f(x,t)$ is transformed to the mapping space $(f(\varsigma(x,t),t))$. The differential operators with coordinate transformation are also mathematically related through the following equations (Farrashkhalvat & Miles, 2003; Rattanadecho, 2008):

$$\frac{\partial}{\partial x} = \frac{\partial}{\partial \varsigma}\frac{\partial \varsigma}{\partial x} = \frac{1}{l-R}\frac{\partial}{\partial \varsigma} \tag{11}$$

$$\frac{\partial}{\partial t} = \frac{\partial}{\partial \varsigma}\frac{\partial \varsigma}{\partial t} + \frac{\partial}{\partial t} = \frac{\partial}{\partial t} - \frac{\dot{R}(1-\varsigma)}{l-R}\frac{\partial}{\partial \varsigma} \tag{12}$$

Using Equations 12 and 13, the moisture and energy transfer equation in the unfrozen layer (Equation 4) can then be transformed to the following:

$$\left\langle \rho C_p \right\rangle_{eff,U}\frac{\partial T_2}{\partial t} = \left\langle \rho C_p \right\rangle_{eff,U}\frac{\dot{R}(1-\varsigma)}{\iota - R}\frac{\partial \mathrm{T}_2}{\partial \varsigma} + \frac{k_{eff,U}}{(\iota - R)^2}\frac{\partial^2 T_2}{\partial \varsigma^2} \tag{13}$$

4.3 Coordinate transformation at the solidification interface

The motion of solidification interface (Equation 5) can also be transformed and is given by:

$$\rho L \varepsilon \frac{dR}{dt} = \frac{k_{eff,F}}{R}\frac{\partial T}{\partial \eta}\bigg|_{x=R} - \frac{k_{eff,U}}{\iota - R}\frac{\partial T}{\partial \varsigma}\bigg|_{x=R} \tag{14}$$

5. Numerical Schemes

In this study, the method of finite differences based on the notion of the control volumes was used. The generalized system of the nonlinear equations (Equations 9, 13, and 14) was integrated over typical control volumes. After integration over each control volume within the computational mesh, a system of nonlinear equations resulted whereby each equation could be cast into a numerical discretization of the generalized conservation equation.

5.1 Heat transport equation in the frozen layer

$$\begin{aligned}\frac{\left\langle \rho C_{peff,F} \right\rangle_{T_{1,i}}^{n+1} T_{1,i}^{n+1} - \left\langle \rho C_{peff,F} \right\rangle_{T_{1,i}}^{n} T_{1,i}^{n}}{\Delta t} &= \frac{\eta \dot{R}}{R}\frac{\left\langle \rho C_{peff,F} \right\rangle_{T_{1,i+1/2}}^{n+1} T_{1,i+1/2}^{n+1} - \left\langle \rho C_{peff,F} \right\rangle_{T_{1,i-1/2}}^{n+1} T_{1,i-1/2}^{n+1}}{\Delta \eta} \\ &+ \frac{1}{R}\frac{1}{\Delta \eta}\left[\left(k_{eff,F}\right)_{T_{1,i+1/2}}^{n+1}\left(\frac{T_{1,i+1}^{n+1} - T_{1,i}^{n+1}}{R\Delta \eta}\right) - \left(k_{eff,F}\right)_{T_{1,i-1/2}}^{n+1}\left(\frac{T_{1,i}^{n+1} - T_{1,i-1}^{n+1}}{R\Delta \eta}\right)\right]\end{aligned} \tag{15}$$

5.2 Heat transport equation in the unfrozen layer

$$\begin{aligned}\frac{\left\langle \rho C_{peff,U} \right\rangle_{T_{2,i}}^{n+1} T_{2,i}^{n+1} - \left\langle \rho C_{peff,U} \right\rangle_{T_{2,i}}^{n} T_{2,i}^{n}}{\Delta t} &= \frac{(1-\varsigma)\dot{R}}{\iota - R}\frac{\left\langle \rho C_{peff,U} \right\rangle_{T_{2,i+1/2}}^{n+1} T_{2,i+1/2}^{n+1} - \left\langle \rho C_{peff,U} \right\rangle_{T_{2,i-1/2}}^{n+1} T_{2,i-1/2}^{n+1}}{\Delta \varsigma} \\ &+ \frac{1}{(\iota - R)}\frac{1}{\Delta \varsigma}\left[\left(k_{eff,U}\right)_{T_{2,i}}^{n+1}\left(\frac{T_{2,i+1}^{n+1} - 2T_{2,i}^{n+1}}{(\iota - R)\Delta \varsigma}\right) - \left(k_{eff,U}\right)_{T_{2,i}}^{n+1}\left(\frac{2T_{2,i}^{n+1} - T_{2,i-1}^{n+1}}{(\iota - R)\Delta \varsigma}\right)\right]\end{aligned} \tag{16}$$

where n is the current iteration index and n +1 is the new iteration index.

5.3 Solidification interface equation

$$\rho_1 L\varepsilon \frac{3R^{n+1}-4R^{n}+R^{n-1}}{2\Delta t} = k_{eff,F}\left.\frac{3T_{1,end}^{n+1}-4T_{1,end-1}^{n+1}+T_{1,end-2}^{n+1}}{2R^{n+1}\Delta\eta}\right|_{x=R} - k_{eff,U}\left.\frac{-3T_{2,0}^{n+1}+4T_{2,1}^{n+1}-T_{2,2}^{n+1}}{2(\iota-R^{n+1})\varsigma}\right|_{x=R} \quad (17)$$

Finally, to obtain values for all stage variables at the marching time, the system of nonlinear equations must be resolved. This procedure was carried out in two distinct stages including the outer and inner iteration phases. During the outer iteration phase, the system of the nonlinear equation is linearized according to the standard Newton–Raphson method. During the inner iteration phase, the system is solved by employing the standard successive overrelaxation method. The conditions for numerical analysis are initial conditions of thermal properties are used to calculate the thermal properties, initial of solidification interface and initial of the distribution temperature determined of a thin layer in frozen layer at the beginning of the process to make it easier to calculate. Grid convergence is 150 grid used to describe the improvement of results using successively smaller cell sizes for the calculations. The fully implicit time discretization finite difference scheme was used to arrive at the solution in time. The time step was 1s and relative error in the iteration procedures of ^{6}-10 was chosen. Additionally, the details regarding numerical discretization of this method can be found in the recent literature.

6. Uncertainties Analysis

When we report a fractional uncertainty of some parameters, U , we write it as

$$U = \frac{\sqrt{D_1^2 + D_2^2 + ... + D_N^2}}{N} \quad (18)$$

where N is the number of cases the measurement is performed and U refers to the fractional uncertainty. If on the other hand, the best estimate of a parameter is determined by making repeated measurements and computing the average value from the multiple trials, the uncertainty associated with each measurement can be determined from the standard deviation, D. Mathematically, the standard deviation can be expressed as

$$D = \frac{\sqrt{\sum_{i=1}^{n}(x_i - \bar{x})^2}}{n-1} \quad (19)$$

where n is the number of times the measurement is performed, x_i corresponds to the i measurement of the parameter x, and is the average value of $\bar{x}$. Typically, the uncertainty is small compared to the measured value, so it is convenient to multiply the fractional uncertainty by 100 and report the percent uncertainty as

Percent Uncertainty = Fractional Uncertainty × 100 (20)

7. Results and Discussion

In this study, the saturated porous packed bed consisted of water and spherical solid particles. The properties used for computations are given in Table 1. Water and ice and two types of particles with the same diameter of 0.15 mm and porosity of 0.385 were considered, i.e. glass and steel beads. The following results show the effects of the type of solid particle and power input on heat transport phenomena within the saturated porous packed bed.

Table 1. All properties used for computations.

Properties	Water	Ice	Glass particle	Steel particle
k	$0.5721e^{0.002T}$	$2.2036e^{-0.004T}$	1.4	$83.693e^{-0.002T}$
c_p	$42068e^{-3E-04T}$	$20558e^{0.0028T}$	0.80	$389.99e^{0.0026T}$
ρ	$1000.7e^{-1E-04T}$	$917.02e^{-1E-04T}$	2500	7870

The computed results from the unsteady problem were extracted and analyzed with the experimental data under various conditions. The percent uncertainty of the experimental data obtained was 7.2.

Figure 4 shows the time variation of the frozen layer thickness for the case of water-glass particle (GB) bed with freezing temperatures T_S = -5 ^{o}C, T_S = -8 ^{o}C, and T_S = -10 ^{o}C. It was observed that the thickness in the case of T_S = -10 ^{o}C grew faster in the solidification process compared with T_S = -8 ^{o}C and T_S = -5 ^{o}C. These results may be explained by considering the latent heat of freezing and heat transfer in the frozen layer. In general, lower freezing temperatures corresponding to the case of T_S = -10 ^{o}C resulted in higher exothermic reaction as the latent heat leading to a higher solidification rate. In addition, at the later stages of the solidification process, the growing rate of the frozen layer decreased due to the resistance to heat transfer from lateral walls to the unfrozen layer. The calculated results were in good agreement with the experi-mental results for the solidification process.

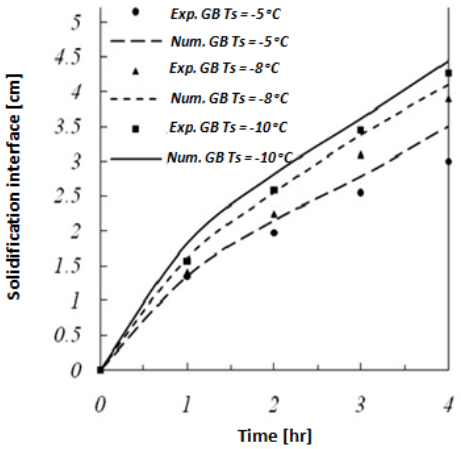

Figure 4. Predicted and experimental solidification interface for the cases of water-glass particle (GB) at freezing temperatures T_S = -5 ºC, T_S = -8 ºC, T_S = -10 ºC.

Figure 5 shows the temperature profiles in the packed bed for the case of the GB bed with T_S = -5 ºC, -8 ºC, and -10 ºC. In general, the temperature in the packed bed dropped faster in the case of T_S = -10 ºC compared with T_S = -8 ºC and T_S = -5 ºC. Furthermore, a lower freezing temperature resulted in faster propagation of the solidification interface for the same duration in every case of T_S. This occurred because of the latent heat and higher heat transfer rate mentioned earlier. The results agree well with the experimental results for the solidification process.

Figure 6 shows the time variation of the frozen layer thickness for the steel particle (Stl) bed with freezing temperatures T_S = -5 ºC, -8 ºC, and -10 ºC. It was observed that the thickness in the case of T_S = -10 ºC was larger in the solidification process compared with T_S = -8 ºC and -5 ºC. These results were due to the latent heat of freezing and heat transfer in the frozen layer. In general, lower freezing temperatures corresponding to T_S = -10 ºC resulted in more latent heat and at the same time led to a higher heat transfer. In addition, although heat transfer resistance increased with time, the growing rate of the frozen layer became greater in the later stages of the process due to the higher thermal diffusivity of steel. The calculated results are in agreement with the experimental results for the solidification process.

Figure 7 shows the temperature profiles in the packed bed for the case of the Stl bed with T_S = -5 ºC, -8 ºC, and -10 ºC. In general, the temperature in the packed bed dropped faster in the case of T_S = -10 ºC compared with T_S = -8 ºC, and T_S = -5 ºC. Furthermore, a lower freezing temperature caused the solidification interface to move faster for the same duration in every case of T_S. This result was observed previously in the case of the GB bed. This is because of the latent heat and higher heat transfer rate as mentioned earlier. In addition, the temperature of the unfrozen zone above 0 ºC decreased more compared with the GB bed due to the large thermal conductivity of steel. Even though the model under-predicts temperatures during the first two hours of the process, the overall results agreed reasonably well with the experimental data.

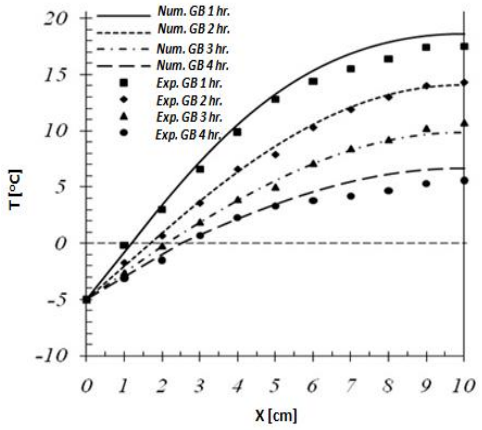

(a) T_S = -5 ºC

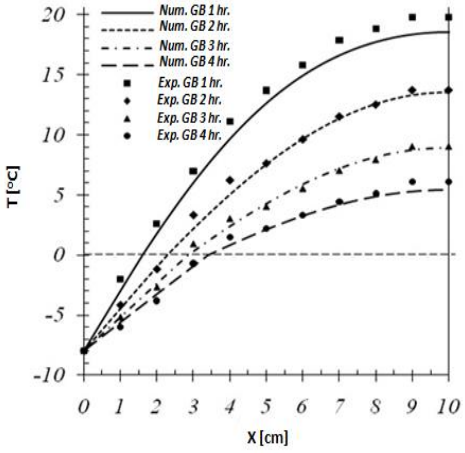

(b) T_S = -8 ºC

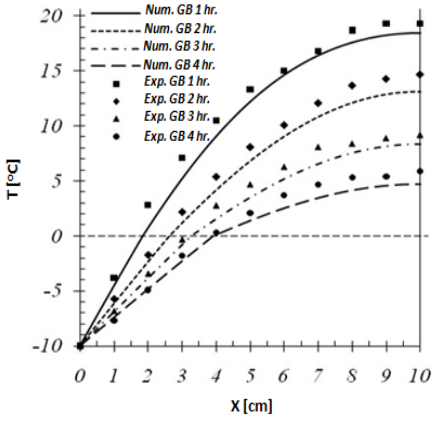

(c) T_S = -10 ºC.

Figure 5. Comparison of the temperature distribution between the predicted and experimental data for the cases of water-glass particle (GB) at freezing temperatures (a) T_S = -5 ºC, (b) T_S = -8 ºC, (c) T_S = -10 ºC.

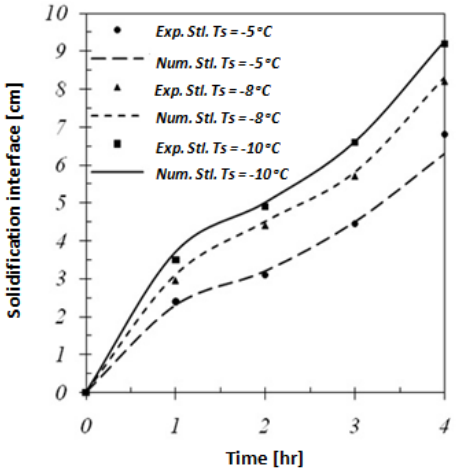

Figure 6. Predicted and experimental solidification interface for the cases of water-steel particle (Stl) at freezing temperatures T_S = -5 ºC, T_S = -8 ºC, T_S = -10 ºC.

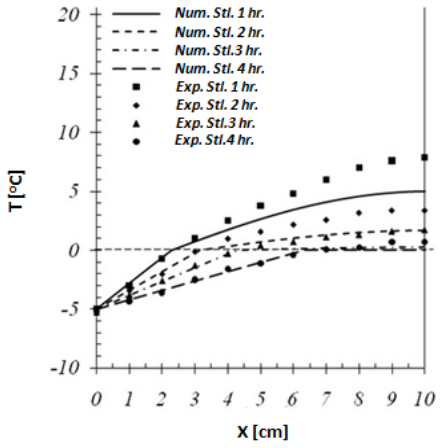

(a) T_S = -5 ºC

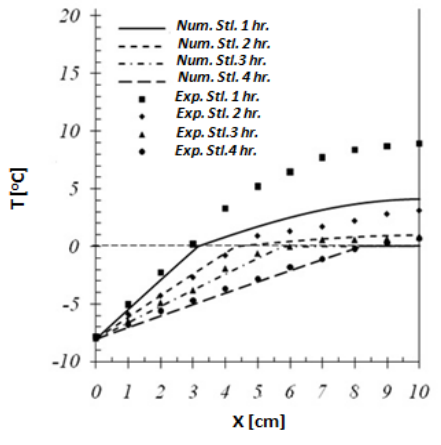

(b) T_S = -8 ºC

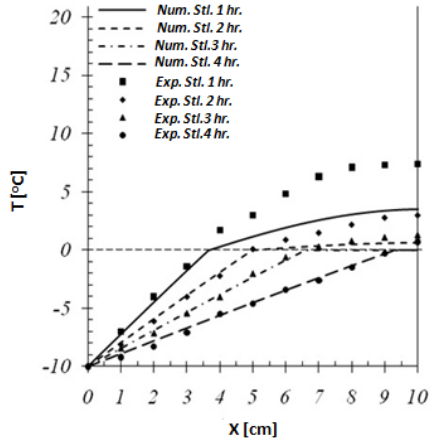

(c) T_S = -10 ºC

Figure 7. Comparison of the temperature distribution between the predicted and experimental data for the cases of water-steel particle (Stl) at freezing temperatures (a) T_S = -5 ºC, (b) T_S = -8 ºC, (c) T_S = -10 ºC.

The time variation of the frozen layer thickness is depicted in Figure 8 for the case of the GB bed and Stl bed at T_S = -8 ºC. It was observed that the thickness in the Stl bed got larger in the solidification process compared with the GB bed. These results were due mainly to the higher thermal conductivity that caused a higher heat transfer rate within the packed bed. Further, at the later stages of the solidification process, the growth rate of the thickness in the case of the Stl bed became partially higher compared with the GB bed due to the fact that steel not only has higher thermal conductivity but also heat capacity.

Figure 9 compares the temperature profiles in the packed beds for the cases of the GB bed and Stl bed at T_S = -8 ºC. In general, the temperature in the packed bed drops faster

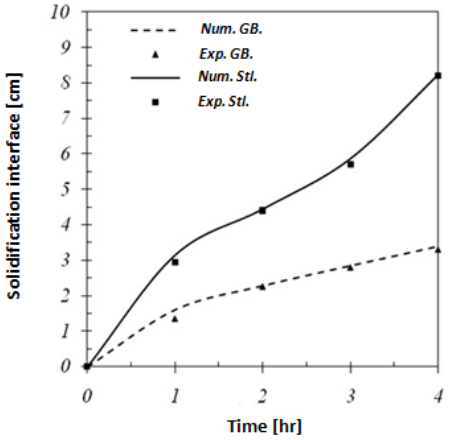

Figure 8. Comparison between the predicted and experimental solidification interface for the cases of water-glass particle (GB) and water-steel particle (Stl) at T_S = -8 ºC

in the case of the Stl bed compared with the GB bed. This is because of the higher thermal conductivity of steel that causes higher heat transfers in the packed bed.

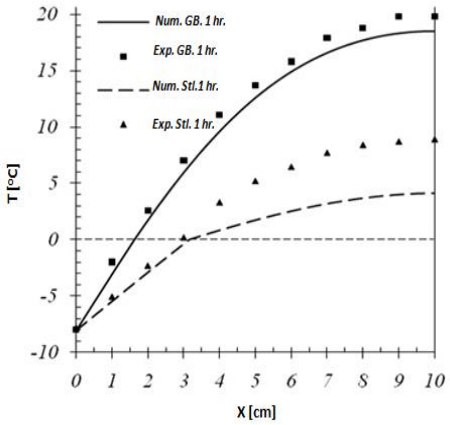

(a) at 1 hr

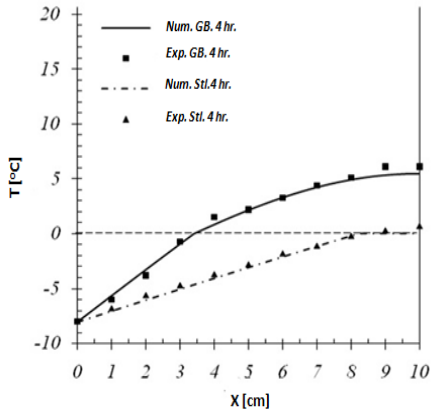

(b) at 4 hr

Figure 9. Comparison between the predicted and measured temperature profiles for the cases of GB and Stl at (a) at 1 h (b) at 4 h with T_S = -8 °C .

8. Conclusions

The solidification process in water saturated porous medium was investigated experimentally and numerically considering beds of solid particles of glass and steel and freezing temperature to obtain quantitative temperature distribution and solidification interface propagation. The one-dimensional solidification model associated with phase change conditions and the coordinate transformation techniques for a moving boundary problem were thoroughly presented. The proposed model is used to predict the solidification interface position and temperature distribution. The numerical prediction and experimental data showed good agreement and thus confirms the mathematical model for a system of glass particles and water. However, for a water-steel particle system, the agreement between predictions and experimental data was not as good since the thermo-physical properties in the unfrozen layer were inadequate.

The errors involved in the process stem from limitations of the numerical methods. The error arisen from the initial solidification interface and initial temperature distribution imposed for a thin layer in frozen layer at the beginning of the process to make it possible to calculate. The differences between the numerical and experimental results are attributed mainly to the heat loss during the experiments and measurement errors. Additional discrepancies may be due to the mathematical model that neglects the effect of natural convection.

Acknowledgements

The authors gratefully acknowledge the Thailand Research Fund (TRF) contract no. RTA5980009 for supporting this research.

References

Beckermann, C., & Viskanta, R. (1988). Natural convection solid/liquid phase change in porous media. *International Journal Heat and Mass Transfer, 31*(1), 35-46.

Celik, I., Hassan, Y., Hughes, D., Johnson, R., & Sommerfeld, M. (1994). *Experimental and computational aspects of validation of multiphase flow CFD codes, FED-Vol. 180*. New York, NY: The American Society of Mechanical Engineers.

Chellaiah, C., & Viskanta, R. (1989). Freezing of water-saturated porous media in the presence of natural convection: Experiments and analysis. *ASME Journal Heat Transfer, 111*(2), 425-432.

Devireddy, R. V., Smith, D. J., & Bischof, J. C. (2002). Effect of microscale mass transport and phase change on numerical prediction of freezing in biological tissues. *ASME Journal Heat Transfer, 124*, 365-374.

Farrashkhalvat, M., & Miles, J. P. (2003). *Basic structured grid generation with an introduction to unstructured grid generation.* Oxford, England: Butterworth-Heinemann.

Frivik, P. E., & Comini, G. (1982). Seepage and heat flow in soil freezing. *ASME Journal Heat Transfer, 104*, 323–328.

Hao, D., Zhonghua, Q., Shuyu, S., & Tao, T. (2014). Adaptive moving grid methods for two-phase flow in porous media. *Journal of Computational and Applied Mathematics, 265*, 139-150.

Hashemi, H. T., & Sliepcevich, C. M. (1973). Effect of seepage stream and artificial soil freezing. *ASCE Mechanics and Foundations Division, 99*, 267–289.

Hosseini, M. J., Ranjbar, A. A., Sedighi, K., & Rahimi, M. (2012). A combined experimental and computational study on the melting behavior of a medium temperature phase change storage material inside shell and tube heat exchanger. *International Communications in Heat and Mass Transfer, 39*, 1416-1424.

Ismail, K. A. R., & Henríquez, J. R. (2000). Solidification of PCM inside a spherical capsule. *Energy Conversion and Management, 41*, 173-187.

Javierre, E., Vuik, C., Vermolen, F. J., & Van der Zwaag, S. (2006). A comparison of numerical models for one-dimensional Stefan problems. *Journal of Computational and Applied Mathematics, 192*, 445-459.

Lu, J., & Zhou, Y. X. (2002). Analytical study on the freezing and thawing processes of biological skin with finite thickness. *International Journal Heat and Mass Transfer, 38*, 319-326.

Ng, K. W., Gong, Z. X., & Mujumdar, A. S. (1998). Heat transfer in free convection-dominated melting of a phase change material in a horizontal annulus. International Communications. *Heat and Mass Transfer, 25*, 631-640.

Olgun, M. C., Medina, M. A., Sanziel, M. C., & Tarzia, D. A. (2007). Behavior of the solution of a Stefan problem by changing thermal coefficients of the substance. *Applied Mathematics and Computation, 190*, 765-780.

Rattanadecho, P. (2004). Experimental and numerical study of solidification process in unsaturated granular packed bed. *Journal of Thermophysics and Heat Transfer, 18*(1), 87-93.

Rattanadecho, P., Aoki, K., & Akahori, M. (2001). A numerical and experimental investigation of the modeling of microwave melting of frozen packed beds using a rectangular wave guide. *International Communications in Heat and Mass Transfer, 28*, 751-762.

Rattanadecho, P., Suttisong, S., & Somtawin, T. (2014). The numerical and experimental analysis of heat transport and water infiltration in a granular packed bed due to supplied hot water. *Numerical Heat Transfer; Part A: Applications, 65*, 1007-1022.

Rattanadecho, P., & Wongwises, S. (2008). Moving boundary-moving mesh analysis of freezing process in water-saturated porous media using a combined transfinite interpolation and PDE mapping methods. *ASME Journal Heat Transfer, 130*, 1–10.

Reston, V. A. (1998). *AIAA Guide for the Verification and Validation of Computational Fluid Dynamics Simulations.* Reston, VA: American Institute of Aeronautics and Astronautics.

Reston, V. A. (1999). *AIAA Assessment of Experimental Uncertainty With Application to Wind Tunnel Testing.* Reston, VA: American Institute of Aeronautics and Astronautics.

Sathaporn, T., Tanongkiat, K., & Atipoang, N. (2008). Heat transfer model of slurry ice melting on external surface of helical coil. *International Communications in Heat and Mass Transfer, 35*, 1335-1339.

Seeniraj, R. V., & Sankara Hari, G. (2008). Transient freezing of liquids in forced flow inside convectively cooled tubes. *International Communications in Heat and Mass Transfer, 35*, 786-792.

Serttikul, C., & Rattanadecho, P. (2007). The numerical of thawing process in phase change slab using variable space grid technique. *Songklanakarin Journal of Science and Technology, 29*(5), 1393-1405.

Sparrow, E. M., & Broadbent, J. A. (1983). Freezing in a vertical tube. *ASME Journal Heat Transfer, 105*, 217–225.

Tan, F. L. (2008). Constrained and unconstrained melting inside a sphere. *International Communications in Heat and Mass Transfer, 35*, 466-475.

Weaver, J. A., & Viskanta, R. (1986). Freezing of liquid-saturated porous media. *ASME Journal Heat Transfer, 108*, 654–659.

Weaver, J. A., & Viskanta, R. (1986). Melting of frozen porous media contained in a horizontal or a vertical cylindrical capsule. *International Journal Heat and Mass Transfer, 29*(12), 1943-1951.

Zhang, X., & Hung Nguyen, T. (1999). Solidification of a superheated fluid in a porous medium: Effects of convection. *International Journal Numerical Methods for Heat and Fluid Flow, 9*(1), 72-91.

Appendix

Nomenclature

C_p	specific heat capacity [J/kgK]
k^p	thermal conductivity in frozen layer [W/mK]
L	latent heat [J/kg]
l	total length [m]
R	length of solidification interface (m)
T	temperature [°C]
t	time [s]
x	coordinate axis [m]

Greek letters

ε	porosity [m^3 / m^3]
ρ	density [kg/m^3]
η, ς	coordinate transformation

Subscripts

0	initial
1, F	frozen layer
2, U	unfrozen layer
eff	effective

Abbreviations

Exp.	experiment
Num.	numerical
Stl.	water-steel particle
GB	water-glass particle